2D Auxetic Metamaterials with Tuneable Micro-/Nanoscale Apertures

Luke Mizzi, Enrico Salvati, Andrea Spaggiari, Jin-Chong Tan, Alexander M. Korsunsky

Supplementary Information

1. Fabrication and Loading of Macroscale Rubber and Kapton Metamaterials

The rubber and Kapton metamaterials were manufactured using direct laser cutting on a Universal® Laser cutting machine. The rubber sheet was 1 mm thick while for the Kapton, a 75 μm thick film was used. The laser pathway was predefined using Ansys® Mechanical 16 and AutoCAD® software and a laser spot size of 300 μm was used. Both systems used the same base geometry, shown in Figure S1 (marked in white), and possess the following geometric parameters: $p = 5$ mm, $s = 0.4$ mm and $w = 0.3$ mm. A 5×7 system of repeating units was used. Following laser cutting, the systems were cleaned under sonication for 10 minutes. The systems were experimentally tested by mounting on a Deben® Micro tensile loading device and stretched in the *y*-direction at a rate of 1.5 mm/min.
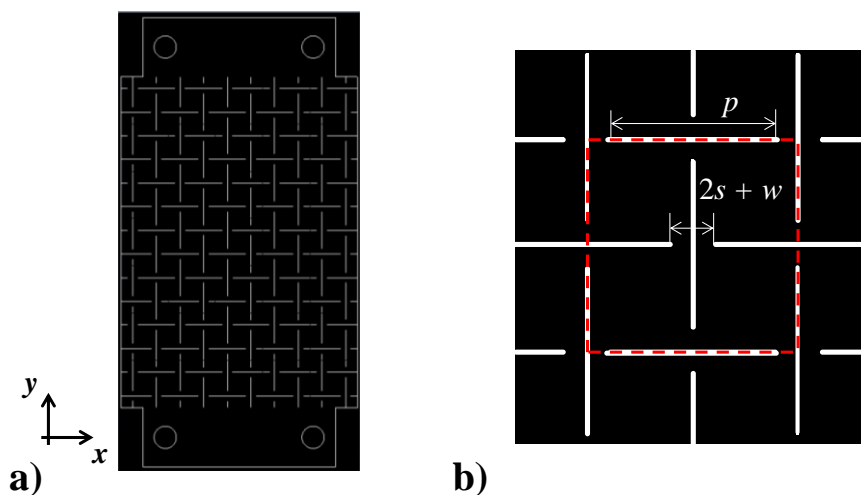

Figure S1: a) Laser pathway for the design of the metamaterial sheet, including the upper and base regions which are clamped to microtensile loader and b) parameters defining the lattice dimensions of the system. The red line marks the representative unit cell of the system.

2. Finite Element Analysis

The FE simulation was conducted using the ANSYS® Mechanical 16 software. A planar equivalent of the FIB-milled system was designed, i.e. the parameters were set at $p = 8$ μm, $s = 300$ nm, $w = 150$ nm and 5×7 repeating units were used. The system was meshed using the PLANE183 element, a higher order 2D 8-noded element with two degrees of freedom at each node and quadratic displacement behavior. The element smart sizing option set at maximum fineness was used to mesh the system which resulted in a minimum element size of $w/3$ at the joint regions of the system. The linear elastic material properties of the system were set to a Young's modulus of 200 GPa and a Poisson's ratio of 0.3. The system was fixed from the upper and lower sides as shown in Figure S2 and a tensile strain of 0.05 was applied in the y-direction. The simulation was conducted under plane-stress conditions using the nonlinear geometric solver. The strains of the central repeating unit of the system were measured for each substep by recording the displacements in the x- and y-directions of each node on the blue dashed lines marked in Figure S2. These strains were then used to calculate the Poisson's ratio of the system.
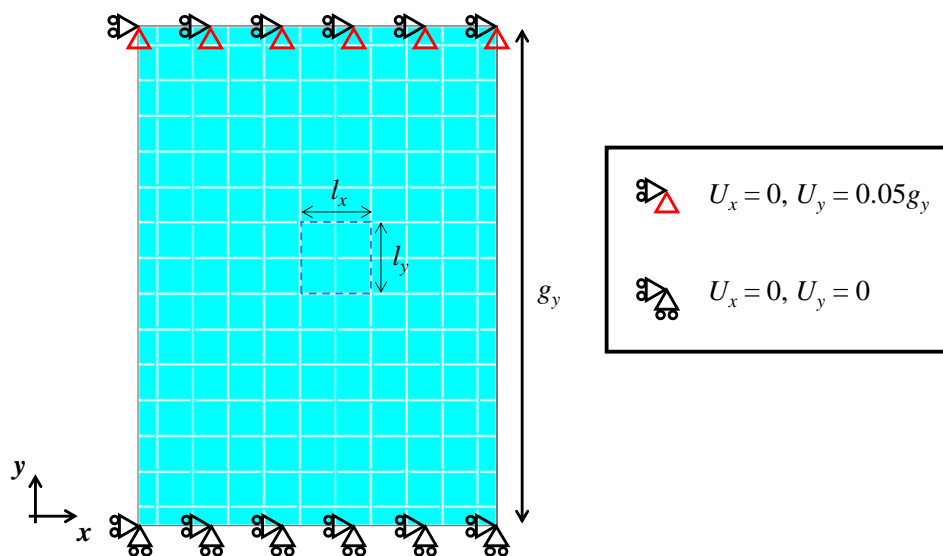

Figure S2: Fixes and loads applied to the FE system and a marked region indicating the section from which the Poisson's ratio of the central repeating unit was measured.

3. Image Analysis of Experimental Results

The Poisson's ratio and pore analysis of the experimental systems were conducted using Matlab. As shown in Figure S3, the displacements of the pore corners (indicated by markers) of the systems were tracked for the image of the central repeating unit and these points were used to calculate the Poisson's ratio of the system in a similar manner to the FE simulation.
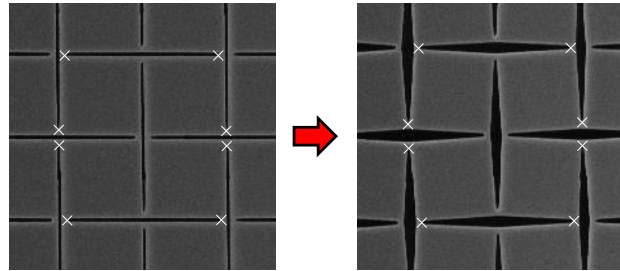

Figure S3: Images of the FIB-milled system with markers indicating the regions of the system which were tracked during the point tracking analysis. The same technique was used for the rubber and Kapton macroscale metamaterials.

The Poisson's ratio of the FIB-milled system was estimated by weighted linear regression of the strain data, considering the resolution error of the marker tracking program. The effect of this error on the final strain values was calculated using error propagation methods. This technique was also extended to the calculation of the Poisson's ratio, as shown in Figure S4 below.
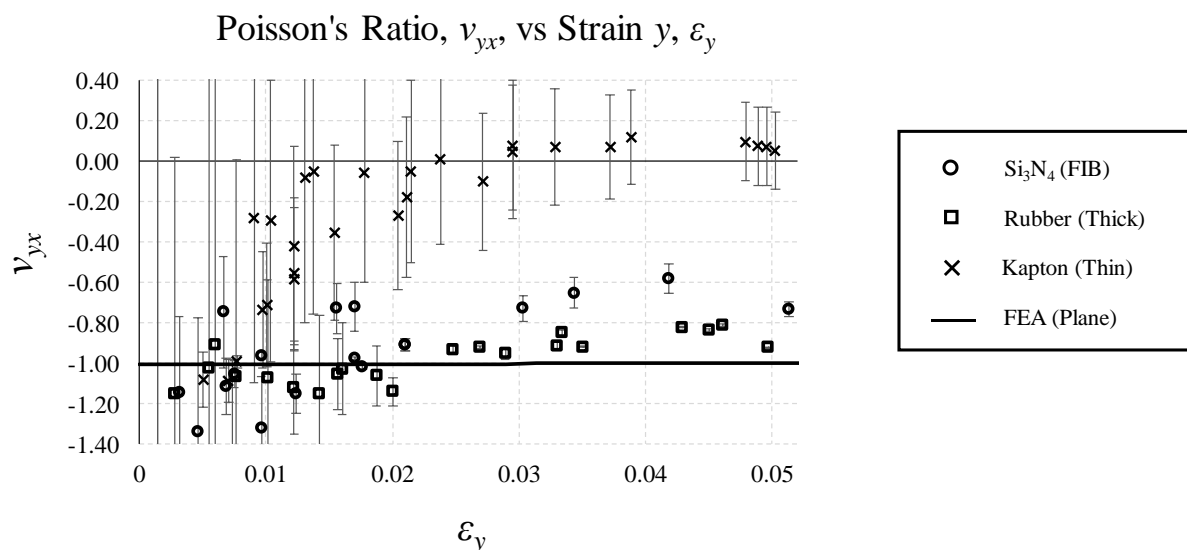

Figure S4: Poisson's ratio vs Strain for each data point with standard deviation (equivalent of Figure 2d in main manuscript).

As one may observe from this plot, the maximum error is observed at small strains in each case. This was to be expected since resolution errors become increasingly less significant as the measured displacement increases, i.e. the resolution error is of a constant magnitude while the displacement values increase with increasing strain. Hence, the higher strain values give a more accurate picture of the Poisson's ratio of these systems.

The analysis of the porosity and aperture shape of the FIB-milled system was also conducted using image analysis techniques. The void area percentage, %A_V, which was defined by the equation below, was calculated using the following steps.

$$\% A_V = \frac{\text{Void Area}}{\text{Total Area of Repeating Unit}} \times 100$$

First the total area of the repeating unit was calculated at all strains based on the readings obtained from the point tracking analysis shown in Figure S3. Then, this region of the SEM image was converted into a binary image using the appropriate threshold value and the number of pixels making up the void area was counted and divided by the total number of pixels in the binary image.

The dimensions of the central pore were measured using a similar tracking technique to the Poisson's ratio analysis as shown in Figure S5a below. These dimensions were then used to find the maximum permissible spherical diameter which can pass through the pore. In order to account for the fact that the system has a non-zero initial porosity, the pore shape was approximated as an irregular hexagon rather than a rhombus as shown in Figure S5b.
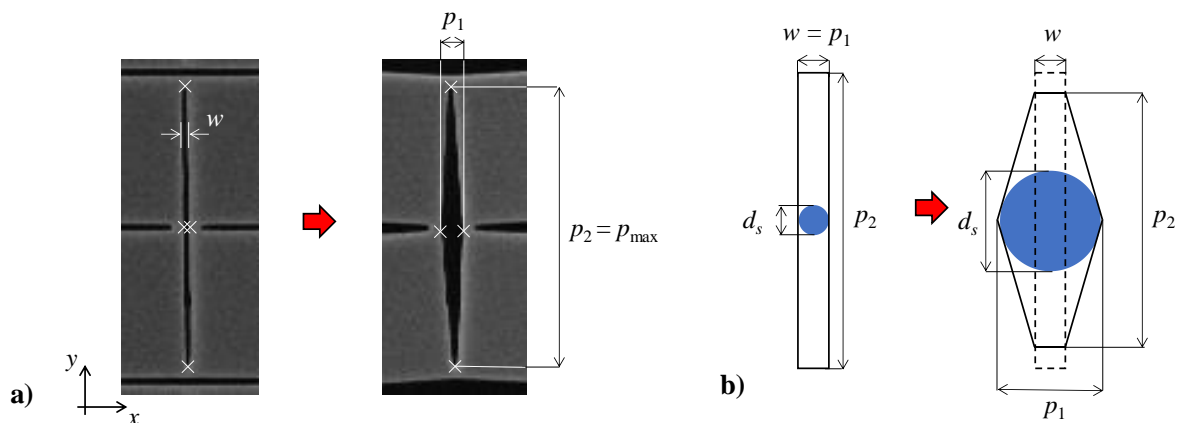

Figure S5: a) Image of tracked pore points in SEM images and b) a sketch showing how the spherical porosity of the system changes with increasing strain.

The parameters w, p_1 and p_2 obtained from the image analysis of the SEM pictures were used to calculate the spherical porosity using the equation below (also shown in the main manuscript):

$$d_s = \sqrt{\left(\frac{p_1}{\dfrac{p_2}{p_1 - w} + \dfrac{p_1 - w}{p_2}}\right)^2 + \left[\left(\frac{p_1}{\dfrac{p_2}{p_1 - w} + \dfrac{p_1 - w}{p_2}}\right)\frac{p_2}{p_1 - w}\right]^2}$$

As shown in Figure S5b, the pore may be approximated as a rectangle when the system is in its undeformed state with area $p_1 \times p_2$ and a d_s value equal to p_1. However, once the metamaterial system opens, the pore transforms into an irregular hexagon, with the corners of the pore retaining a minimum thickness w at all times during deformation. Using the equation above, one may accurately estimate the d_s value of the system once it opens. Obviously, given the fact this system undergoes only small deformations, the d_s value is extremely similar to the p_1 dimension of the pore in the cases investigate here. However, in the event of a similar system deforming at large strains where the main pore dimensions p_1 and p_2 become of comparable length, the d_s value would become significantly smaller than the p_1 value and hence this equation covers even the possibility of a system such as the one studied here reaching its fully-opened form.